Available online at www.sciencedirect.com

jmr&t Journal of Materials Research and Technology

journal homepage: www.elsevier.com/locate/jmrt

Original Article

Analysis of microstructure, mechanical properties, and wear performance of NiTi alloy fabricated by cold metal transfer based wire arc additive manufacturing

Gaofeng Liu [a], *Shihui Zhou* [a], *Pengyu Lin* [a,b,*], *Xuemei Zong* [c], *Zhikai Chen* [c], *Zhihui Zhang* [a], *Luquan Ren* [a]

[a] *Key Laboratory of Bionic Engineering (Ministry of Education), and College of Bionic Science and Engineering, Nanling Campus of Jilin University, 5988 Renmin Street, Changchun 130025, PR China*

[b] *Department of Planning, First Automotive Works (FAW)-Volkswagen Co. Ltd., Anqing Road No. 5, Changchun 130012, PR China*

[c] *State Key Laboratory of Intelligent Manufacturing of Advanced Construction Machinery, Xuzhou 221004, PR China*

ARTICLE INFO

Article history:
Received 9 May 2022
Accepted 10 July 2022
Available online 16 July 2022

Keywords:
NiTi alloy
Superelasticity
Wire arc additive manufacturing
Cold metal transfer
Microstructure
Mechanical properties

ABSTRACT

In this work, wall-shaped NiTi components were fabricated by cold metal transfer (CMT) based wire arc additive manufacturing (WAAM) with optimized depositing speed. The microstructure, mechanical properties, and wear performance of the as-fabricated specimens along the building direction, together with their correlations were investigated in-depth. Coarse columnar grains were refined gradually with the increase of wall height. An equiaxed microstructure was obtained in the upper region. The Ni_4Ti_3 precipitates were distributed in the matrix. The microhardness, critical stress, and elongation increase monotonously with the increase of wall height. Plastic deformation, together with wear-induced work hardening is the main form of wear, which is mainly hindered by the superelasticity of NiTi alloys. Good homogeneity of the microstructure, mechanical properties, and wear resistance is obtained due to the CMT process with optimized depositing speed, indicating that this technique provides great potential to make novel NiTi flexible structures.

* Corresponding author.
E-mail addresses: linpengyu2000@gmail.com, pengyu.lin@faw-vw.com (P. Lin).

https://doi.org/10.1016/j.jmrt.2022.07.068

1. Introduction

NiTi shape memory alloys (SMAs) have attracted attention in automotive, aerospace, and biomedical fields, due to their excellent superelasticity, shape memory properties, biocompatibility and corrosion resistance [1]. Owing to their superelasticity, these alloys can be bent or stretched for large deformation, but will return to the original shape after the release of external load. Moreover, the shape memory property restores their shape from the deformed state to the earlier undeformed state by changing the temperature. Nevertheless, the inherent poor machinability limited the development of geometrically complex components for conventionally processed NiTi alloys [2]. In general, NiTi alloys are usually fabricated via conventional approaches, e.g. casting followed by machining and powder metallurgy, which always face low efficiency, high reject rate, high processing cost, and worse dimensional stability, owing to severe brittleness and poor machinability of NiTi alloys. As a result, conventionally fabricated NiTi components have simple geometries, such as wires, plates, and bars, restricting severely practical applications of NiTi SMAs [3]. In order to produce NiTi alloy more efficiently, additive manufacturing (AM) is preferred due to its high material utilization rate and high geometrical complexity.

The most commonly used AM technologies for fabricating NiTi parts are powder-based AM technologies, for instance, selective laser melting (SLM) and laser metal deposition (LMD) [4,5]. These studies mainly focused on the relationship between process parameters, microstructure, phase transformation behavior and functional properties [6]. It was found that powder-based AM technologies generally can provide a better surface finish and dimensional accuracy, which are normally required for NiTi devices. As a result, the powder-based AM technologies, especially SLM, of NiTi alloys have been frequently addressed [7,8]. Nevertheless, it is worth noting that powder-based AM technologies are apt to generate porosity since hollow particles often exist due to the gas entrapment during the manufacturing process [9]. Besides the gas entrapment, the unfavorable balling effect and lack of fusion are also responsible for the formation of porosity. On the other hand, the low processing efficiency of powder-based AM technologies is another important factor limiting its application in fabricating large component.

In recent years, some researchers focused on the fabrication of NiTi alloys by wire arc additive manufacturing (WAAM), which is an efficient, low-cost additive manufacturing method that uses electric arc as a heat source to melt the feeding wire [10]. In addition, although the surface finish and dimensional accuracy of WAAM-fabricated NiTi alloys is not as high as those fabricated by SLM or LMD, this method is highly mature in industries like automobile body-in-white (BIW) manufacturing, due to its high automation rate (For instance, combination of industrial robots and electric arc torches is widely used in the BIW body shops of Volkswagen) and desired output stability. Generally, the composition of wire feedstock is more uniform than powder materials, and wire feedstock carries fewer surface impurities since the specific surface area of wire materials is much smaller than powder materials. Existing studies mainly focused on the microstructure, phase transition temperature and mechanical properties of deposited materials. Wang et al. [11] reported NiTi walls fabricated by WAAM using separate pure Ni and Ti wires, showing that the evolution of microstructure, transformation temperature and mechanical properties was affected by the extraordinary thermal history during the depositing process. Besides separate wire feedings of Ni and Ti, The commercial available NiTi wire is also used in previous studies [12], where gas tungsten arc welding (GTAW) based WAAM was employed to evaluate the temperature and heat flow modelling. Moreover, Resnina et al. [13] reported a Ni-rich (50.9 at.%) NiTi wall of five layers fabricated by gas

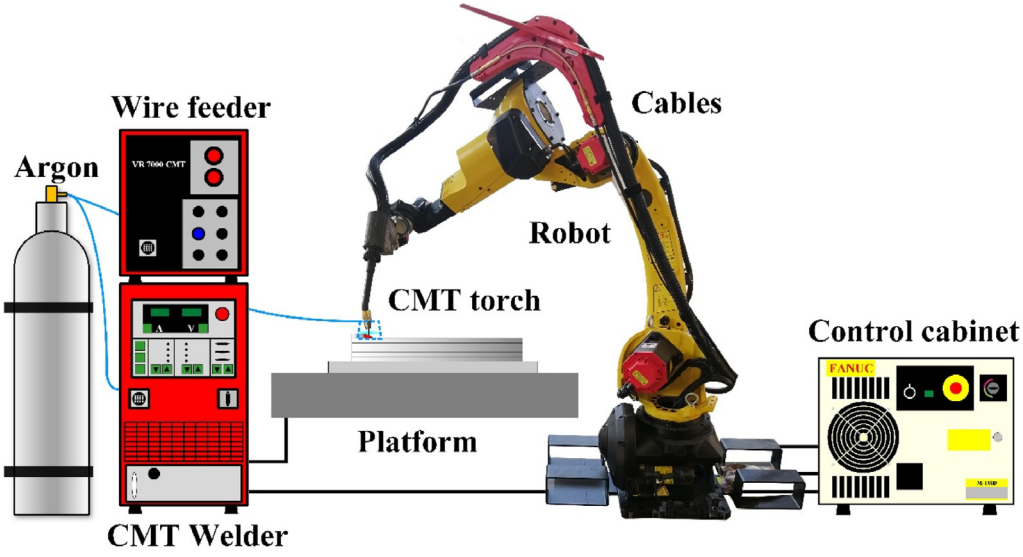

Fig. 1 – The CMT system for NiTi alloy fabrication.

Table 1 – Chemical compositions of the NiTi wire and substrate (wt.%).

Material	Ni	Co	Cu	Cr	Fe	Nb	C	H	O	N	Ti
Wire	55.74	0.005	0.005	0.005	0.005	0.025	0.040	0.001	0.038	0.001	Bal.
Substrate	55.74	0.005	0.005	0.005	0.012	0.005	0.035	0.001	0.040	0.001	Bal.

metal arc welding (GMAW) and evaluated the related shape memory effect.

Cold metal transfer (CMT) is a modified GMAW, originally developed by Fronius International GmbH for dissimilar welding in the automotive field. Due to its low heat input and unique transition mode, higher solidification rate is obtained, together with uniform microstructure, less splash and high surface quality. CMT fabricated NiTi walls exhibited good metallurgical bonding and few defects, together with varying appearance of Ti_2Ni/Ti_4Ni_2O precipitates [14]. Good mechanical and functional properties, especially high ductility, were obtained. Furthermore, Zhang et al. [15] reported that CMT fabricated NiTi walls exhibited superior superelastic properties, with the recovery rate of >94%, indicating that CMT provides great potential to make NiTi parts.

Although the above works studied in-depth the relationship between process parameters, microstructure, martensitic transformation, mechanical properties and shape memory effect of NiTi alloy, more work is highly required to make novel NiTi smart structures, especially by innovative methods like CMT. The present work aims to explore the preparation of NiTi walls by CMT with varying depositing speed. The microstructure, phase transformation, mechanical properties, and wear performance of the fabricated NiTi walls were analyzed in-depth. It is also the first time to study the effect of depositing speed on CMT-fabricated NiTi alloy.

2. Experimental procedure

2.1. CMT process

The NiTi walls were deposited on a NiTi substrate using the custom-built CMT system, as demonstrated in Fig. 1, comprising a FANUC industrial robot (M-10iD12), a Fronius CMT welder (TransPlus Synergic 4000, with RCU5000i controller), a working platform, VR 7000 CMT wire feeding system, FK4000R cooling system, and shielding gas system (99.99% pure argon). The range of welding current and voltage is 3–400 A and 14.2–34.0 V, respectively.

Table 2 – The optimized process parameters during the CMT process.

Process parameters	Value
Substrate	NiTi
Thickness of substrate	10 mm
Torch traveling speed (cm/min)	20, 30, 40
Wire feeding speed (m/min)	3, 4, 5, 6, 7, 8
Arc length	15 mm
Shielding gas	Pure argon, 99.99%
Gas flow speed	20 L/min
Torch angle	90°
Post flow duration	90s

The Ni-rich (55.74 wt.%) NiTi wire with the diameter of 1.2 mm was used as feeding material. A NiTi plate in the dimensions of 200 x 100 x 10 mm^3 was used as the depositing substrate. Their chemical compositions are summarized in Table 1, respectively. The XRD result (Fig. 2a) indicates that the NiTi wire is mainly in austenite phase at room temperature, with no obvious secondary phase detected. Fig. 2b shows the transformation behavior of the NiTi wire as characterized by differential scanning calorimetry (DSC). Multiple transformation peaks were detected, probably due to the heterogeneity of NiTi wire.

The optimized process parameters during the CMT process were summarized in Table 2, where the varying torch traveling speed and wire feeding speed were listed. It is well known that the depositing speed during the CMT process is to large extent determined by the torch traveling speed and wire feeding speed. In order to explore the effect of the depositing speed on CMT

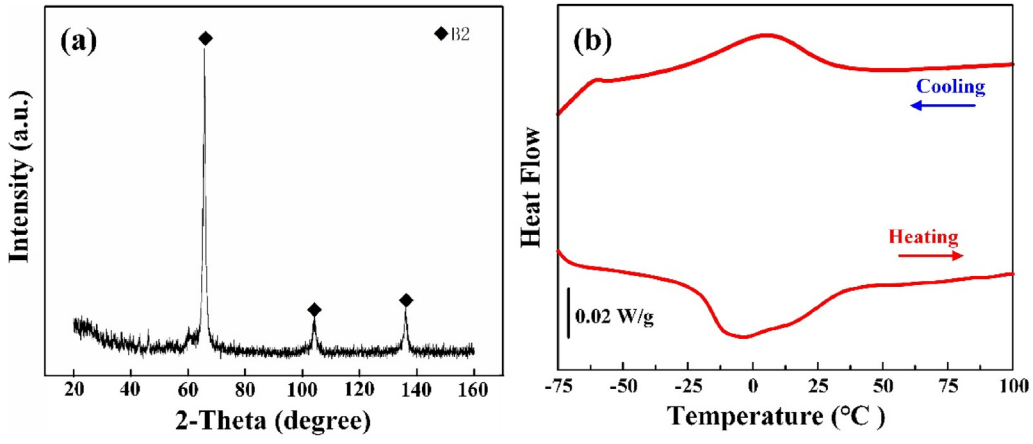

Fig. 2 – Characterization of the NiTi wire. a. XRD, b. DSC.

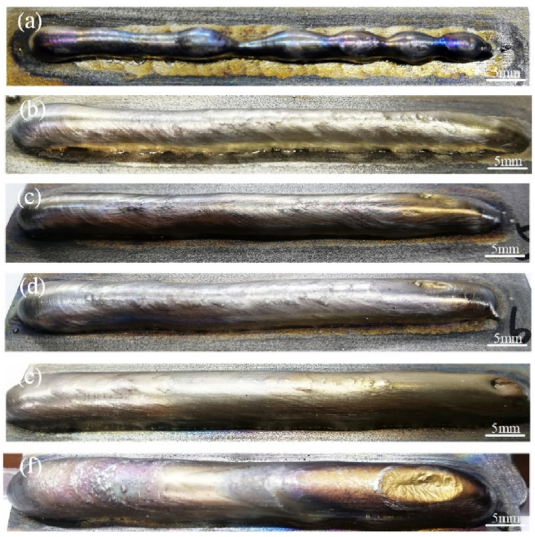

Fig. 3 – Macroscale morphology of the CMT fabricated walls with varying feeding speed, while keeping the depositing speed = 20 cm/min unchanged. a–f. Feeding speed = 3, 4, 5, 6, 7, and 8 m/min, respectively.

fabricated NiTi alloy, different combination of torch traveling speed and wire feeding speed was designed to fabricate NiTi walls, while keeping other process parameters unchanged.

No delamination phenomenon occurred as the deposition progressed. A wall-shaped component with 15 layers was fabricated using the CMT system. Tensile properties along vertical (building) direction of the CMT fabricated NiTi walls were characterized.

2.2. *Characterization*

The microstructure of CMT fabricated NiTi walls was investigated using an optical microscope (OM, ZEISS-Scope AI), a scanning electron microscope (SEM, JSM-IT500A) equipped with the energy-dispersive X-ray spectrometer (EDS). X-Ray diffraction (XRD, D/Max 2500 PC, Rigaku) with Cu Kα radiation was employed to study the phase composition at room temperature. The Vicker's hardness of the specimens was examined using the microhardness instrument (Huayin, HVS-1000) with the load of 200 g and dwell time of 15 s. Mechanical properties were characterized using the tensile testing system (Instron 1121), with the loading rate of 1 mm/min. The fracture morphology after tensile test was characterized by SEM. The

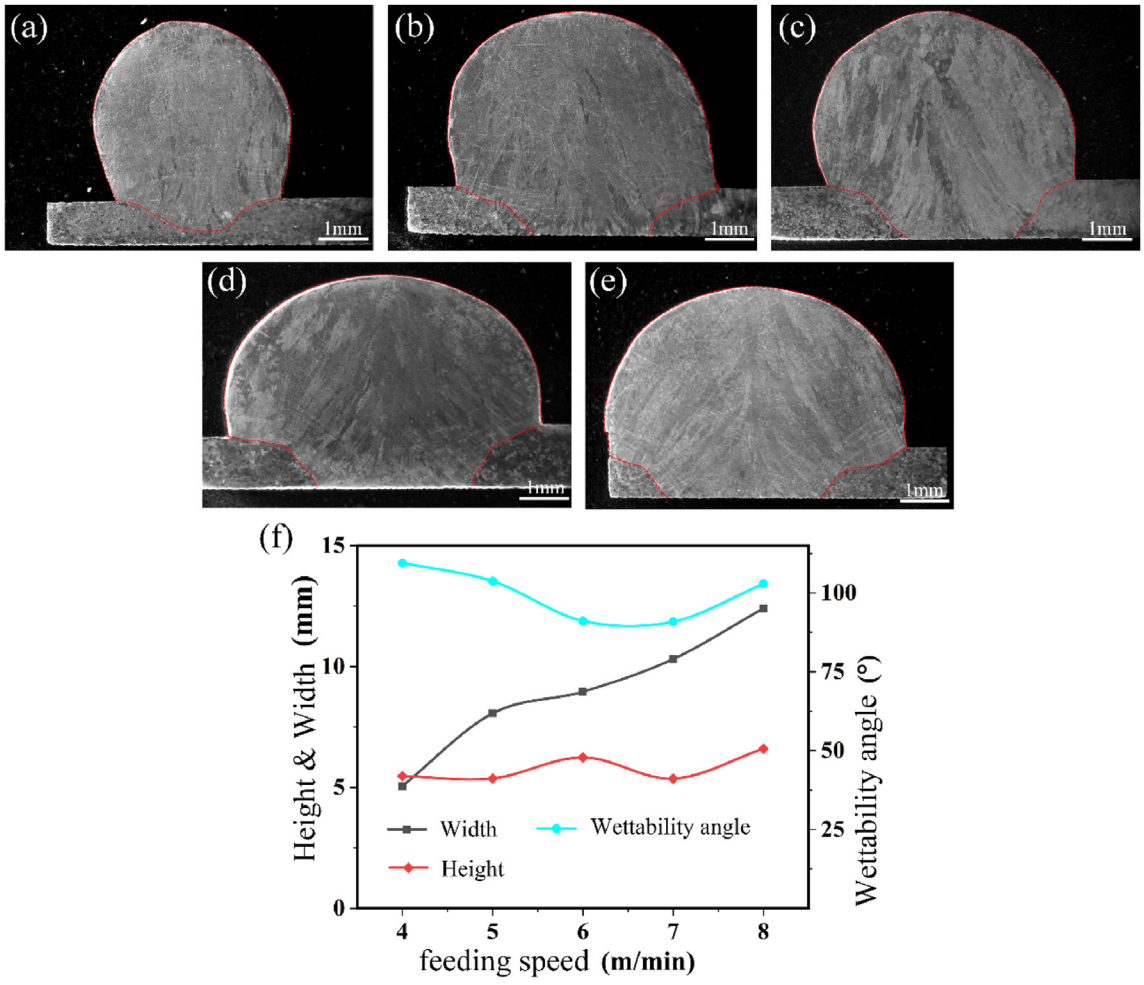

Fig. 4 – Cross-sectional SEM of the CMT fabricated walls in Fig. 3. a–e. Feeding speed = 4, 5, 6, 7, and 8 m/min, respectively; f. Height, width and wettability angle of a-e.

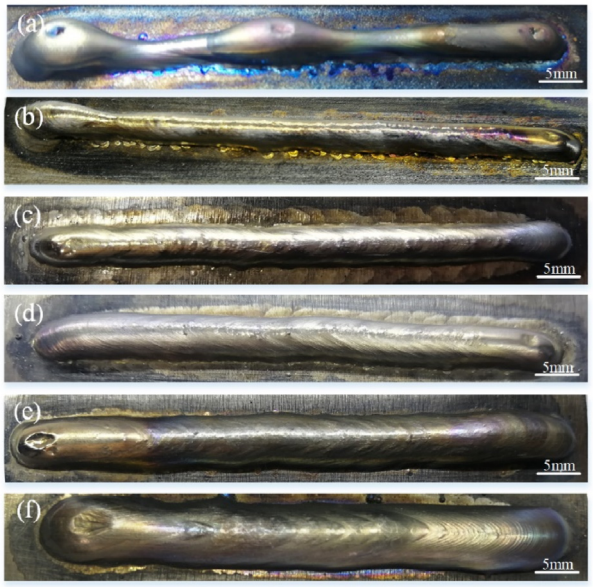

Fig. 5 – Macroscale morphology of the CMT fabricated walls with varying feeding speed, while keeping the depositing speed = 30 cm/min unchanged. a–f. Feeding speed = 3, 4, 5, 6, 7, and 8 m/min, respectively.

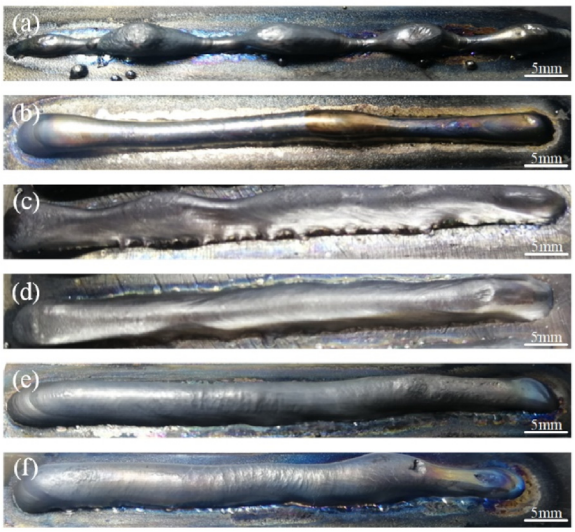

Fig. 7 – Macroscale morphology of the CMT fabricated walls with varying feeding speed, while keeping the depositing speed = 40 cm/min unchanged. a–f. Feeding speed = 3, 4, 5, 6, 7, and 8 m/min, respectively.

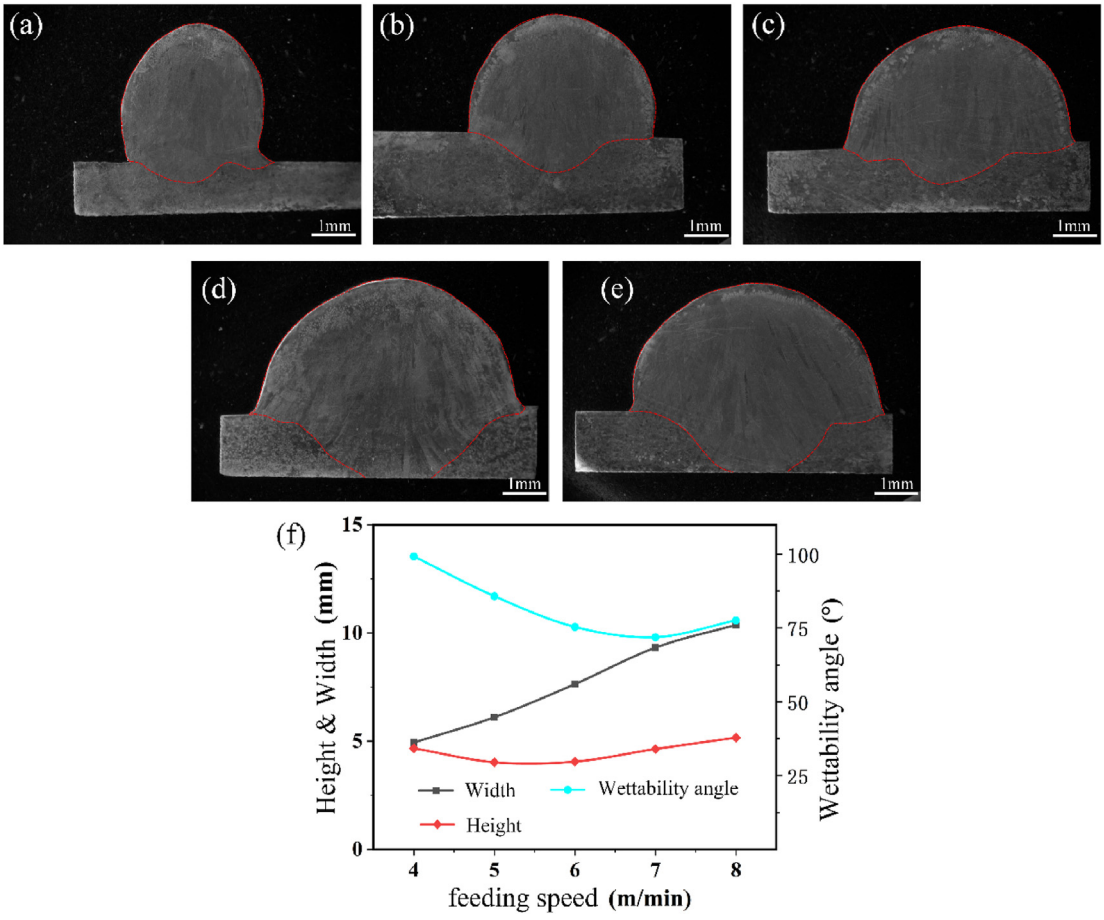

Fig. 6 – Cross-sectional SEM of the CMT fabricated walls in Fig. 5. a–e. Feeding speed = 4, 5, 6, 7, and 8 m/min, respectively; f. Height, width and wettability angle of a-e.

phase transformation behavior was characterized by differential scanning calorimetry (DSC, Discovery DSC 25) with a cooling/heating rate of 10 °C.min^{-1} between −80 and 100 °C. Wear behavior was characterized using a wear tester (UMT-5, Bruker), with the wear time of 10 min, wear speed of 5 mm/s, and wear load of 5, 10, 20 N, respectively.

3. Results and discussion

3.1. *Effect of the depositing speed on CMT fabricated NiTi walls*

In order to improve the microstructure and properties of NiTi alloys fabricated by CMT, previous studies focused mainly on the relationship between microstructure, phase transformation and properties, while keeping the process parameters, including depositing speed, unchanged [14]. Although, as indicated by Yu et al. [14], the wire feeding speed was changed slightly, while keeping the torch traveling speed constant, such a change cannot be regarded as the study on depositing speed. In the case of CMT, the depositing speed is mainly dependent on two factors, i.e. wire feeding speed, which affects mainly material supply, and on the other hand, torch traveling speed, which affects mainly fabrication. In the case of mass production, both wire feeding speed and torch traveling speed are main process parameters, since they are directly associated not only with the quality of parts, but also with the takt time of production. In this work, NiTi walls were fabricated with different combination of wire feeding speed and torch traveling speed, while keeping other process parameters unchanged, in order to obtain good optimization for depositing speed.

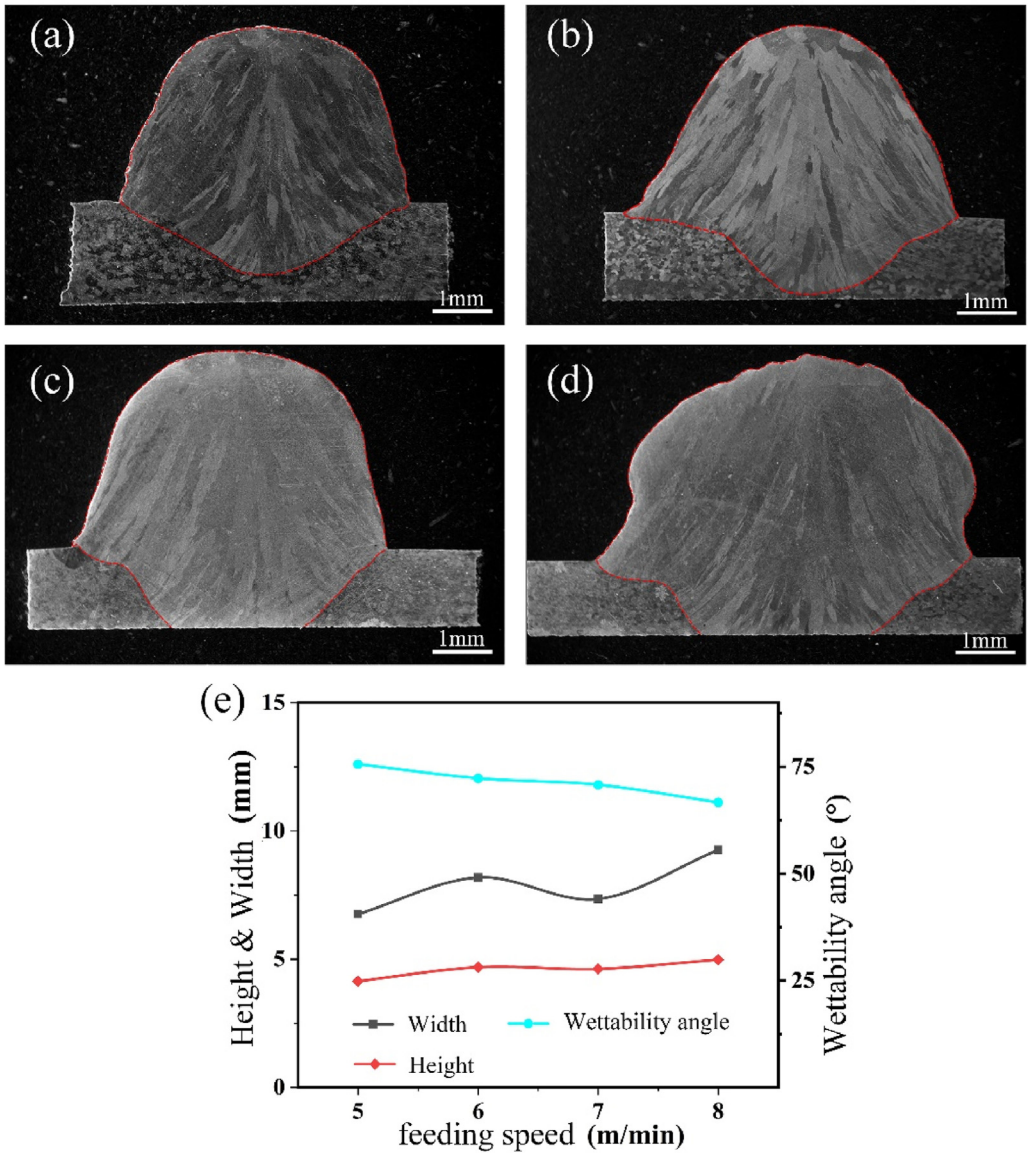

Fig. 8 – Cross-section SEM of the CMT fabricated walls in Fig. 7. a–d. Feeding speed = 5, 6, 7, and 8 m/min, respectively; e. Height, width and wettability angle of a-d.

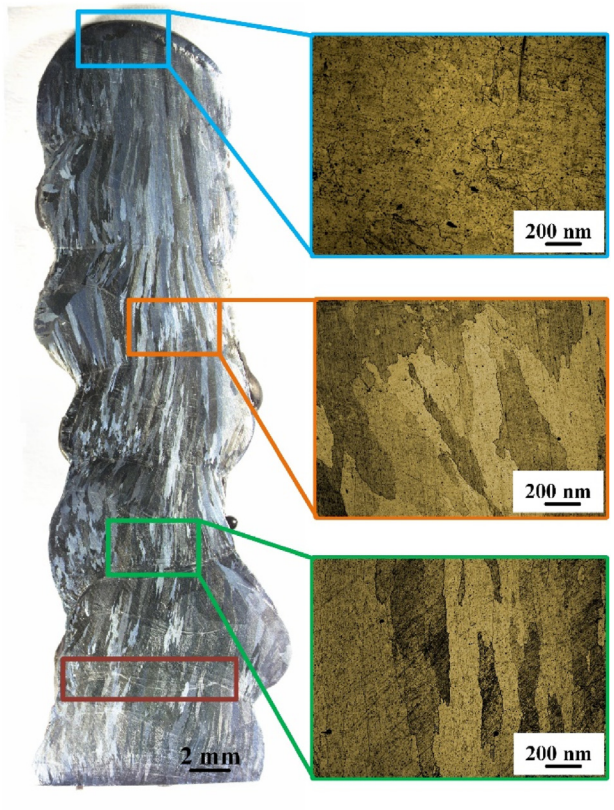

Fig. 9 – Cross-section view of the as-deposited NiTi wall, with microstructure in upper, middle, lower regions, respectively.

Figs. 3–8 show the macroscale and cross-sectional morphologies of the CMT fabricated NiTi walls with different combination of wire feeding speed and torch traveling speed. Figs. 4f, 6f, and 8e show that, while keeping the torch traveling

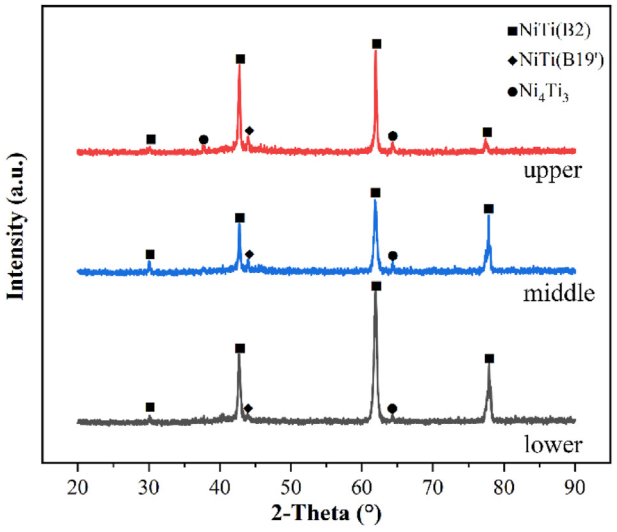

Fig. 10 – XRD patterns of samples in the lower, middle and upper regions of NiTi walls.

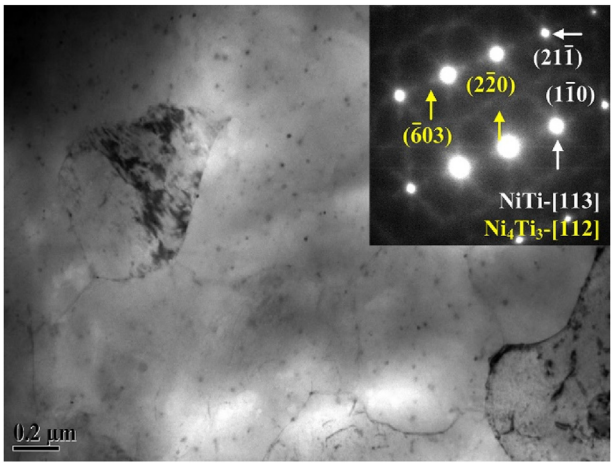

Fig. 11 – TEM image of NiTi walls, with the SAED pattern as an insert.

speed unchanged (20, 30, 40, respectively), the width of NiTi walls exhibits an increasing tread with the increase of wire feeding speed, mainly due to more material supply as wire feeding speed increases. However, such a trend is undermined with the increase of torch traveling speed.

Meanwhile, the height of NiTi walls shows moderate fluctuation, with the change of wire feeding speed. It might be ascribed to the reason that, although more heat is transferred to the melt pool with the increase of wire feeding speed, leading to higher width together with lower height, this effect is offset by more material supply due to the increase of wire feeding speed. Consequently, the fluctuation of height occurred owing to the competition between heat flow and material supply. It is noteworthy that, with the increase of torch traveling speed, the fluctuation of height is undermined.

Besides height and width, the wettability angle of NiTi walls are also summarized in Figs. 4f, 6f, 8e. It is found that the wettability angle of NiTi walls shows a decreasing trend with the increase of torch traveling speed. Generally, the wettability of WAAM is associated with the combined effect of height, width, and wettability angle, as indicated by Yang et al. [16]. The combination of smaller wettability angle, higher width and lower height can lead to superior wettability. Therefore, as demonstrated by the morphology, defects, height, width, and wettability angle of NiTi walls, it is suggested that, in this work, the combination of torch traveling speed = 30 cm/min and wire feeding speed = 6–7 m/min is most optimized for the CMT process.

Furthermore, while torch traveling speed = 40 cm/min, the morphology of all the NiTi walls shows extensive defects, indicating that even with varying wire feeding speed, obvious defects for NiTi walls are inevitable as torch traveling speed increases further. It is well known that the amount of heat input along the building direction is reduced with the increase of torch traveling speed. When torch traveling speed increases up to 40 cm/min in this work, the low heat input cannot enable effective fabrication of the NiTi walls. Therefore, as demonstrated by the above results and analysis, the change of

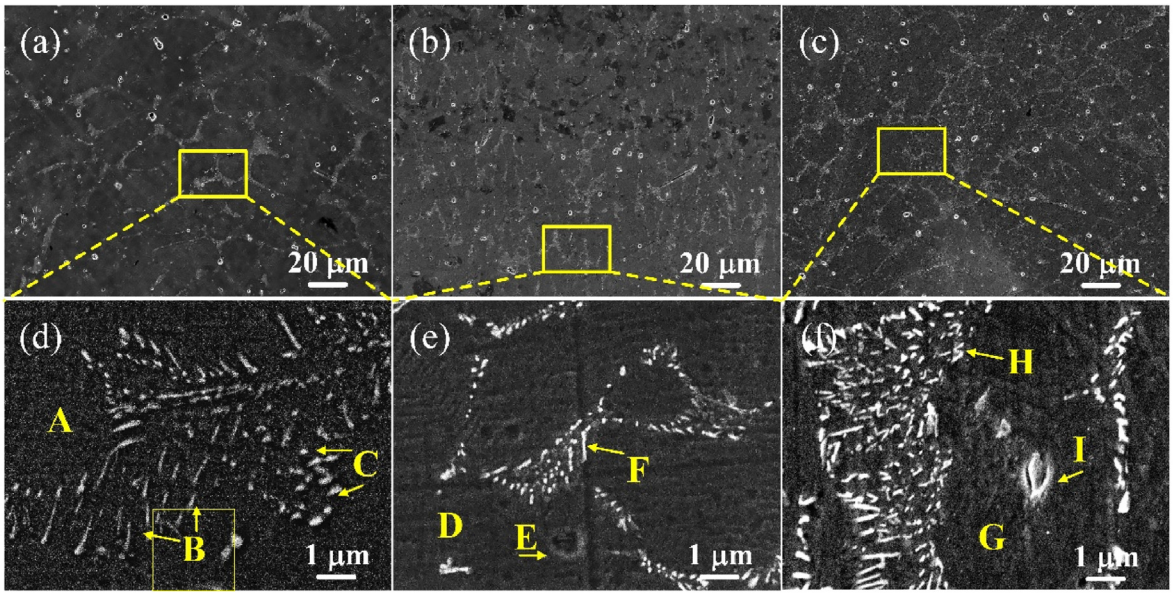

Fig. 12 – SEM images of the lower, middle, and upper regions of CMT fabricated NiTi walls. a–c. Lower, middle, and upper regions, respectively; d–f. Selected areas with higher magnification from a-c.

torch traveling speed shows more pronounced influence on CMT-fabricated NiTi walls than the change of wire feeding speed.

3.2. *Microstructure characterization*

Fig. 9 shows the microstructure diagram along the building direction of the NiTi walls fabricated with the combination of torch traveling speed = 30 cm/min and wire feeding speed = 7 m/min. An equiaxed microstructure can be observed in the upper region. As a comparison, in the middle and lower regions, the distinct columnar microstructure can be observed. In all the regions, obvious pores and cracks cannot be observed. The overlap zone can be seen in the red loop. Besides the upper region, the surface microstructure in the middle and lower regions also exhibits the equiaxed microstructure, as indicated by the blue loops. The microstructure of NiTi wall, which is deposited layer by layer, is mainly dependent on the thermal history during the CMT process, since varying thermal gradient G and grain growth rate R are obtained in different regions. When depositing the first 2–5 layers in the CMT process, the heat was primarily conducted to the NiTi substrate. As a result, a large thermal gradient G was created, leading to formation of the columnar grain structures, which continued to grow epitaxially due to the reheating by deposition of the next layer. Thus, in the lower region, coarse columnar grains are driven by the large thermal gradient during layer-by-layer deposition, which is the typical microstructure of metallic materials fabricated by the WAAM process [17].

After the first several layers, as the deposition process continued, thermal gradient and cooling rate reduced gradually due the pre-heating effect of previous depositions [18]. Besides, owing to the movement of heat source and the deposited layers with accumulated heat, the direction of heat flow was deviated and thereby columnar grains with zigzag grain boundaries were obtained. It is worth noting that as compared with the lower region, the grain size in the middle region reduced, probably due to less heat from the subsequent depositions. Therefore, in the upper region, the last deposited layer had no subsequent thermal cycle conditions, together with the pre-heating effect of previous depositions, which contributed to formation of the equiaxed microstructure in the upper region.

The phase composition as characterized by XRD, collected at room temperature, is shown in Fig. 10. The samples in the upper, middle, and lower regions are mainly in B2 austenite phase at room temperature. Moreover the Ni_4Ti_3 intermetallic phase is detected. No additional phase is detected in any of the upper, middle and lower regions. As demonstrated by the peak intensity of Ni_4Ti_3 phase, the content of Ni_4Ti_3 phase increases with the height of NiTi walls. This is because of the intrinsic thermal cycle conditions during the CMT process, which enables the metastable Ni_4Ti_3 to decompose into stable Ni_3Ti precipitates [19,20]. Nevertheless, Ni_4Ti_3 phase in the upper region remains generally due to the absence of

Table 3 – EDS results of chemical compositions at each area marked in Fig. 12.

at.%	A	B	C	D	E	F	G	H	I
Ni	51.07	54.23	51.74	51.11	47.60	48.07	51.15	49.49	43.86
Ti	48.93	45.77	48.26	48.89	52.40	51.87	48.85	50.51	56.14

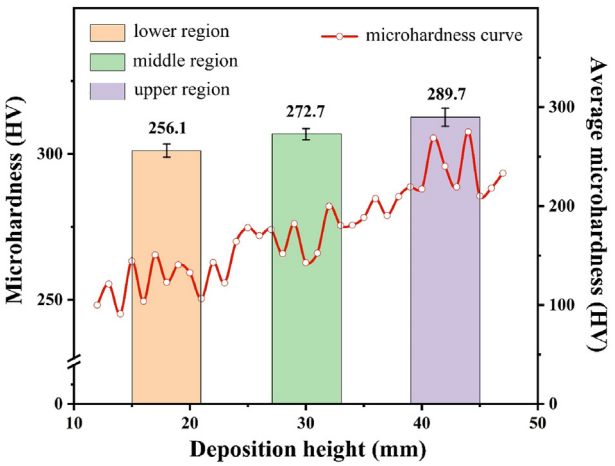

Fig. 13 – Evolution of microhardness along the building direction of NiTi walls.

subsequent thermal cycle conditions so that the content of Ni_4Ti_3 phase in the upper region is higher than both the middle and lower regions.

Fig. 11 is a TEM image of the NiTi walls with the SAED pattern as an insert, indicating that extensive precipitated particles, in appearance of dot and needle, distributed along wavy dislocation line or behind bending dislocations. As shown by the SAED pattern, the precipitated particles are only composed of Ni_4Ti_3. The Ni_4Ti_3 phase is a common strengthening phase in NiTi alloys, as indicated in previous study [21]. It is worth noting that some precipitated particles along the dislocation line are larger in size and higher in density than other ones, indicating that the nucleation and growth of precipitates occurred heterogeneously during the CMT process. The main reason for such behavior can be ascribed to the repeated precipitation process during fabrication [22]. In this work, such behavior is mainly caused by thermal cycle conditions during the layer-by-layer CMT deposition.

Fig. 12 shows SEM images of the lower, middle, and upper regions of CMT-fabricated NiTi walls. The dot/needle-like precipitated particles, distributed in the matrix, can be observed, which is in good agreement with TEM. In order to compare the content of elemental Ni and Ti, EDS results of chemical compositions, at each area marked in Fig. 12, are summarized in Table 3. Wang et al. [23] showed that the content of Ni and Ti changed obviously, together with the evolution of precipitated phase in the matrix, with the variation of NiTi wall height. As a comparison, in this work, the content of Ni and Ti changes moderately with varying wall height, mainly due to the optimization of depositing speed

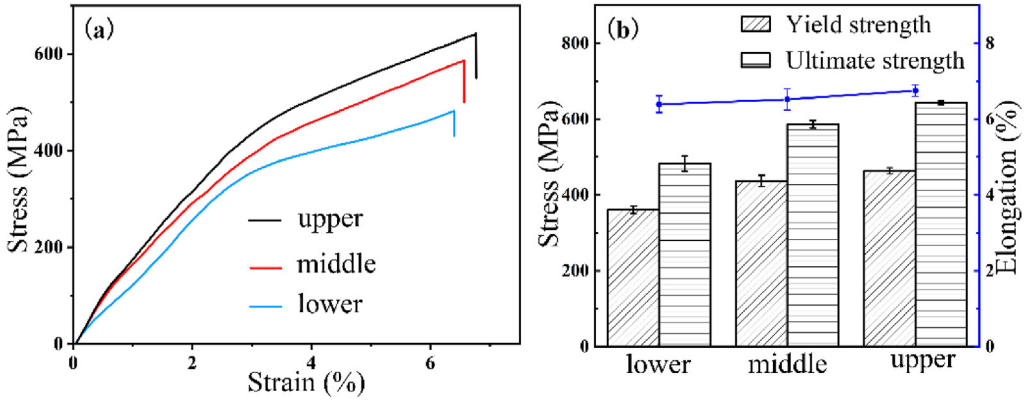

Fig. 14 – Tensile properties of the lower, middle, and upper regions of NiTi walls.

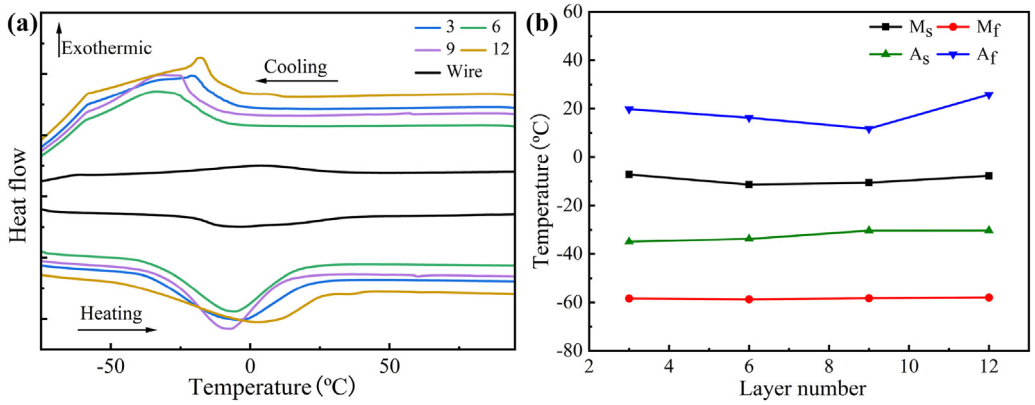

Fig. 15 – DSC results for forward and reverse martensitic phase transformation temperatures of the lower, middle, and upper regions of NiTi walls.

Table 4 – Value of yield strength, ultimate strength and elongation of the lower, middle and upper regions of NiTi walls.

Wall height	Yield strength	Ultimate strength	Elongation
Upper	463.4	642.7	6.75
Middle	436.9	586.2	6.52
Lower	360.4	482.5	6.39

and intrinsic merit of CMT process (good heat management), indicating that the microstructure of CMT-fabricated NiTi walls exhibits higher homogeneity.

3.3. *Mechanical properties*

Fig. 13 depicts the microhardness evolution along the building direction of the NiTi walls. The microhardenss increases gradually with the increase of the wall height. The average hardness in the lower, middle and upper regions are around 256 HV, 273 HV and 290 HV, respectively, with moderate fluctuation. The result is mainly attributed to the evolution of microstructure and precipitation effects. On one hand, as grain size decreases, finer grains contain more grain boundaries and dislocation, showing higher resistance to stress than coarse grains. As aforementioned, the grain size deceases with the increase of wall height, indicating that more grain boundaries and dislocation is obtained in middle and upper regions, which is in good agreement with the distribution of microhardness along the building direction. On the other hand, presence of the Ni_4Ti_3 phase in the microstructure plays a pivotal role in affecting mechanical properties of NiTi walls. Due to the varying thermal cycle conditions along the building direction during deposition, the content of Ni_4Ti_3 precipitates increases with the increase of wall height, providing more

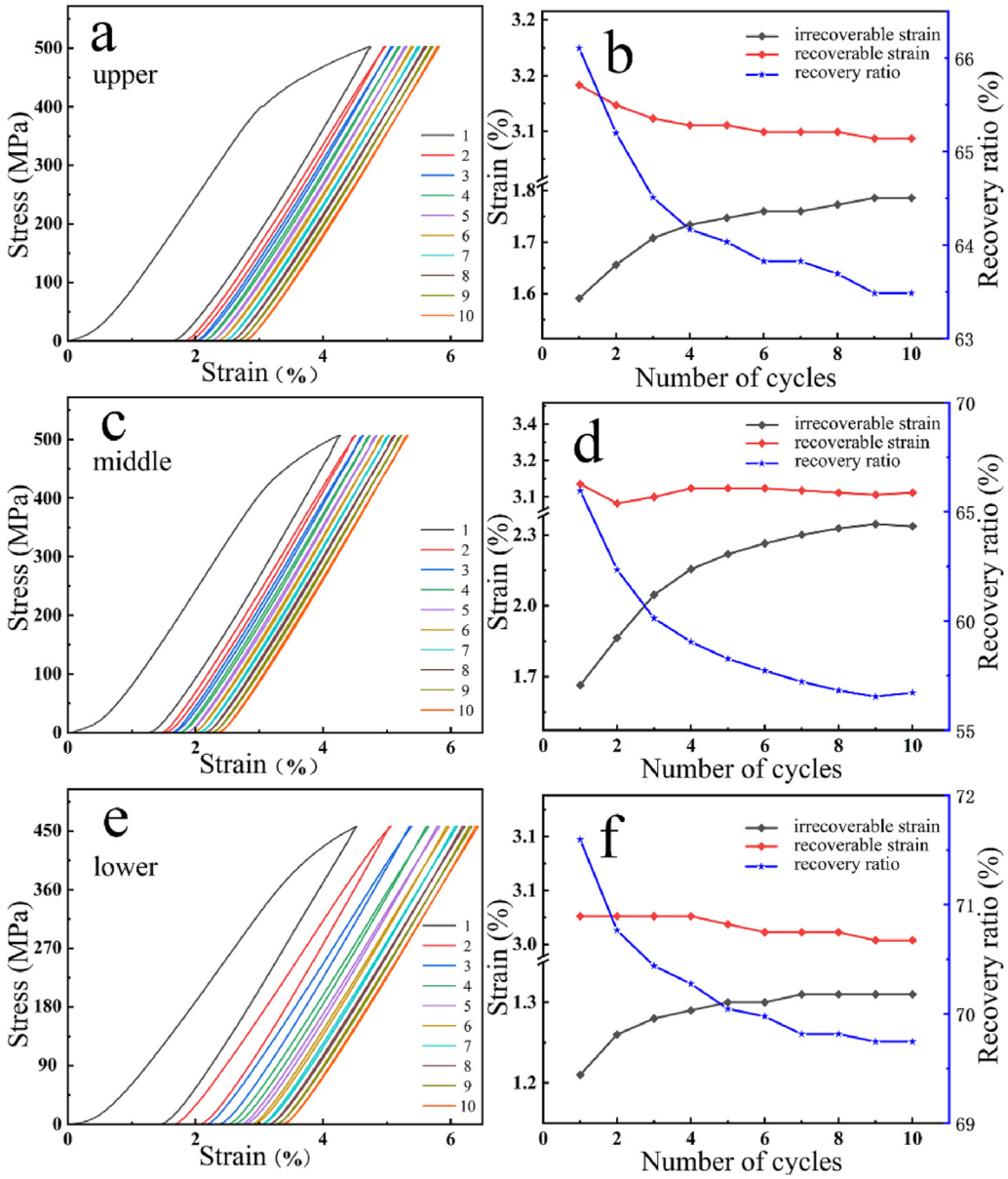

Fig. 16 – The response to load/unload cycles of lower, middle, and upper regions of NiTi walls, with the cumulative cyclic evolution of recovery ratio and irrecoverable strain. a, b. Upper region; c, d. Middle region; e, f. Lower region.

precipitation strengthening effect. As a result, the microhardness in middle and upper regions is increased partly by presence of the precipitates. Besides, owing to the stress-induced martensite transformation by microhardness testing, the microhardness of the produced B19' phase is lower than that of the B2 matrix, leading to the fluctuation of hardness value [24]. The change of microhardness along the building direction was also reported in previous studies [11,14], showing that the microhardness of the upper region was increased by around 42% and 45%, respectively, as compared with the lower region. However, in this work, such trend is undermined, with the increase of 13% obtained, indicating that the distribution of microhardness is more homogeneous. The main reason could be ascribed to the higher microstructure homogeneity, originating from optimization of the depositing speed.

The tensile properties of the lower, middle, and upper regions of NiTi walls are shown in Fig. 14. Yield strength, ultimate strength, and elongation increase with the increase of wall height, respectively, as summarized in Table 4. It is well known that the critical stress decreases with the increase of M_s temperature [25]. The stress-induced martensitic transformation occurs easily while the M_s temperature gets close to ambient temperature, leading to the decrease of critical stress. The martensitic transformation temperatures (MTTs) of NiTi alloys depend highly on the chemical composition, especially the Ni content in the matrix [26]. The M_s temperature decreases by around 20 °C with the increase of only 0.1 at.% Ni content [27]. However, as shown in Fig. 15, only moderate change and fluctuation of the Ms temperature is obtained with different wall height. Thus, it is suggested that, in this work, the change of MTTs associated with the chemical composition is not the main factor for the variation of mechanical properties. Two reasons are suggested as follows. Firstly, the gradual decomposition of Ni_4Ti_3 in the middle and lower regions contributes to the decrease of critical strength, since Ni_4Ti_3 is a main strengthening phase in the matrix. Secondly, according the Hall–Petch relationship, with the increase of wall height, the grain size is reduced gradually, leading to the higher critical stress. Moreover, the elongation is improved mainly due to the smaller-sized columnar grains and equiaxed microstructure with the increase of wall height.

3.4. *Superelasticity*

The superelastic responses of the lower, middle and upper regions of NiTi walls under tension mode are shown in Fig. 16. For all the tested samples, an obvious irrecoverable strain (ε_{ir}) is observed in the first cycle, due to the plastic deformation and residual martensite during mechanical loading [15]. Nevertheless, ε_{ir} increases obviously in the next 5 cycles, while reaching gradually to a stable state with the increasing number of cycles. To the contrary, the recovery ratio decreases significantly in the first 6 cycles, followed by reaching gradually to a stable state, owing to the accumulation of dislocation density and plastic deformation caused by the martensitic phase transformation [8]. Although the martensitic transformation during loading is recoverable, part of the martensite in the matrix is retained due to the imposed stress field and dislocation. Finally, the content of residual martensite is stabilized gradually as the cyclic loading/unloading test proceeds, which explains the evolution of ε_{ir} and recovery ratio [10]. Besides, the change of recovery ratio may be associated with the precipitates in the matrix [28]. The generation of precipitates, such as Ni_4Ti_3 and Ti_2Ni, changes the ratio of Ni/Ti in the matrix, thereby affecting the superelasticity of NiTi alloys.

As compared with the lower region, the middle and upper regions exhibit higher recovery ratio, which originates mainly from the evolution of microstructure with varying wall height. With the increase of wall height, the microstructure is refined gradually, with smaller-sized columnar grains and even equiaxed grains. In general, WAAM-fabricated NiTi alloys exhibit intrinsic microstructural heterogeneity along the building direction, leading to distinct local mechanical behavior. Lower regions with coarse, columnar grains are expected to deform more easily than the middle and upper regions. Therefore, more loss of superelasticity occurs in lower region [29], impairing the complete superelastic recovery of NiTi alloys. In this work, due to the improved microstructural homogeneity, the recovery ratio of the lower, middle and upper regions of NiTi walls is changed moderately, indicating that optimization of the depositing speed has a pronounced influence on the superelasticity of CMT-fabricated NiTi alloys.

Furthermore, both the recoverable strain and recovery ratio increase moderately with the increase of wall height, under the same loading cycles, indicating that the shape

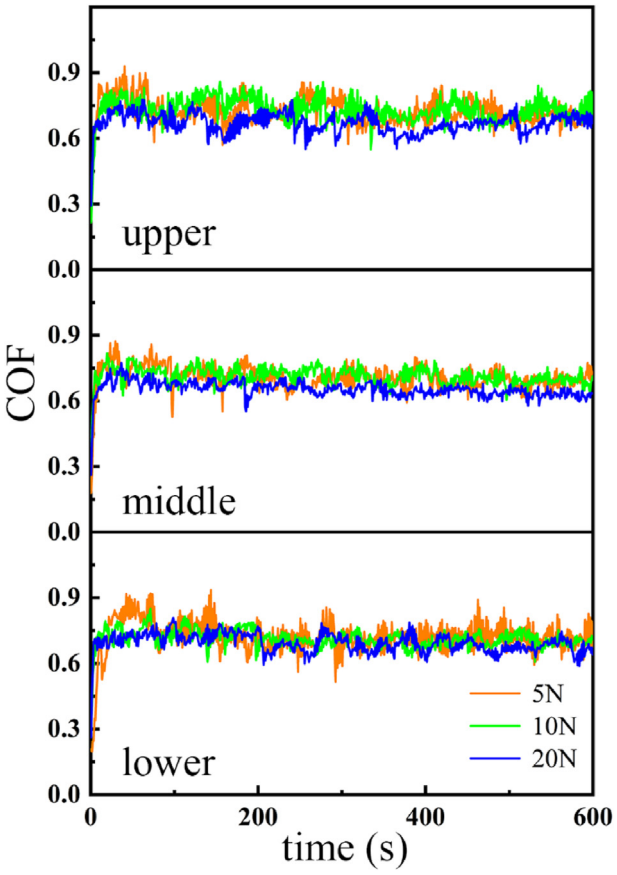

Fig. 17 – Coefficient of friction of the lower, middle, and upper regions of NiTi walls with varying load.

memory property is affected to same degree with varying wall height. However, with respect to the moderate change (<10%) of recovery ratio, obvious distinction in shape memory property along the building direction is not observed. This is because of the improved microstructural homogeneity originating from optimization of the depositing speed, indicating that distribution of the shape memory property is more homogeneous along the building direction and optimization of the depositing speed could act as a process method to tailor the homogeneity of shape memory property of CMT-fabricated NiTi walls as a whole.

3.5. *Tribological performance*

It is well known that the tribological performance of NiTi alloys is dependent on not only hardness and ductility, but also MTTs, work hardening, crack nucleation and propagation resistance, material defects, and etc. [30]. As summarized in Fig. 17, the coefficient of friction (COF) of the lower, middle, and upper regions of NiTi walls with varying load is compared. Owing to the optimization of depositing speed, the CMT-fabricated NiTi walls in this work has no obvious cracks and porosity, as demonstrated in Figs. 3, 5, 7, and 12. Besides, the microstructure, microhardness, and mechanical properties, especially ductility, exhibit good homogeneity with varying wall height, leading to the moderate change of COF for the lower, middle and upper regions.

Nevertheless, COF decreases gradually with the increase of wall height, while keeping the load = 5, 10, and 20 N, respectively. On one hand, the microhardness increases with the increase of wall height, enabling the material surface to hold material transfer more stably. On the other hand, higher ductility could enhance the toughness and the ability to stop, or at least retard, microcracking during wear [31]. It is worth noting that, in the case of NiTi alloys, the B19' martensite in the matrix could be preferentially re-orientated to adapt to the deformation strain, releasing the stress concentration around the crack tip and thereby hindering the propagation of cracks. As a result, due to the combination of higher microhardness, better mechanical properties (critical stress and elongation), and higher content of B19' phase (as demonstrated by XRD), the upper region exhibits superior anti-wear property to the lower and middle regions.

Furthermore, the COF fluctuation of the middle region is more stable than that of the lower and upper regions, indicating that a stable friction behavior is obtained for the

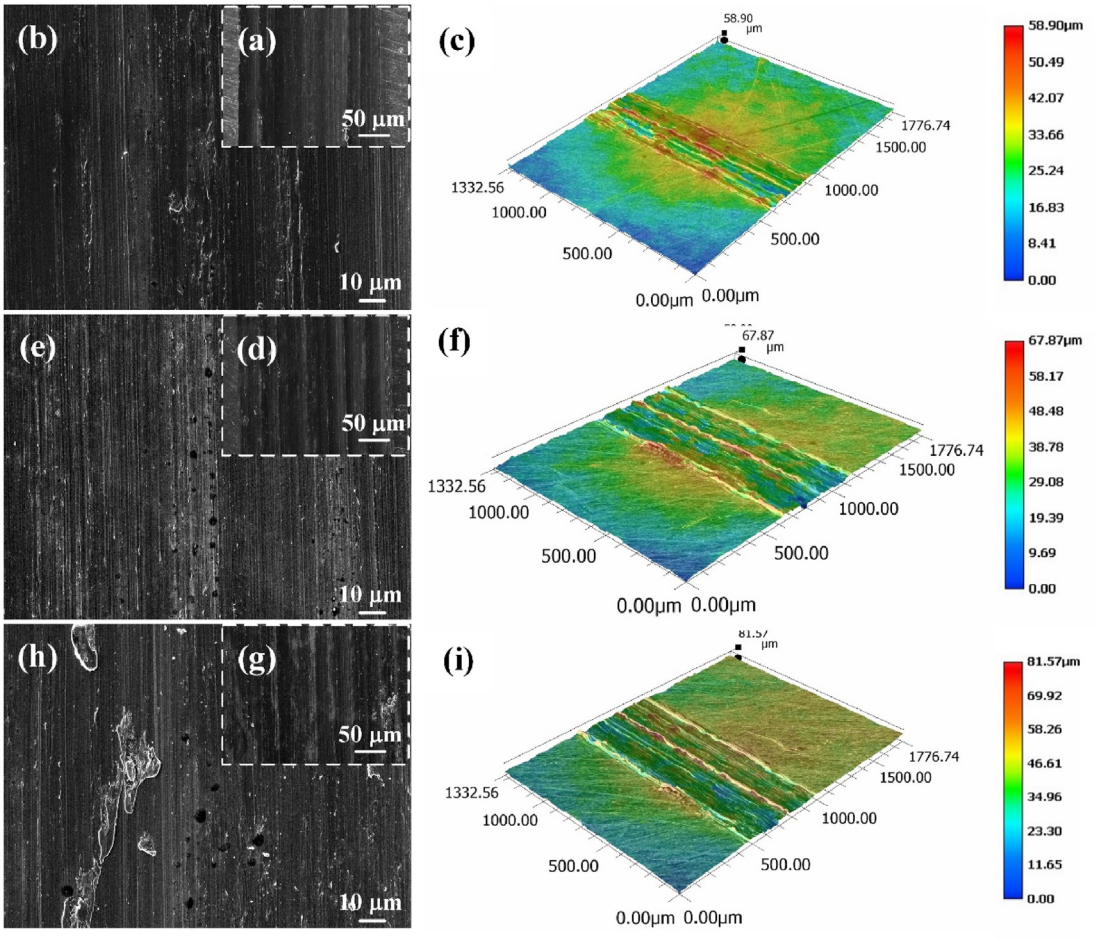

Fig. 18 – Wear morphology of the middle region of NiTi walls with varying load. a-c. Low magnification, high magnification, and 3D image, respectively, with load = 5 N; d-f. Low magnification, high magnification, and 3D image, respectively, with load = 10 N; g-i. Low magnification, high magnification, and 3D image, respectively, with load = 20 N.

middle region. Such phenomenon might be ascribed to two main reasons. Firstly, in the lower region, the inferior mechanical properties cannot hold stably the material transfer during wear, leading to stronger COF fluctuation. Secondly, in the upper region, the competition between the re-orientation of the B19' phase, which releases the stress concentration, and the stress-induced martensitic transformation of the B2 phase, which increases the elastic contact area and reduces the normal stress, is inevitable, as indicated by the cyclic COF fluctuation of the upper region, especially when higher load is applied.

The wear morphology of the middle region of NiTi walls with varying load is shown in Fig. 18, indicating that the depth of the scratch increases with the increase of load. Materials are accumulated on both sides of the scratch, meanwhile obvious cutting is not observed on the surface. Consequently, plastic deformation is the main form of wear, together with wear-induced work hardening, followed by crack nucleation and propagation. Therefore, the superelasticity of NiTi alloys seems to play an important role in practical applications associated with tribology conditions. The varied conditions, such as friction at high or lower loading, could be considered to investigate the effect of superelasticity on wear resistance to surface damage in the follow-up work.

4. Conclusions

In this work, the evolution of microstructure, mechanical properties and wear behavior of CMT-fabricated NiTi alloys, with optimization of the depositing speed (including torch traveling speed and wire feeding speed) were studied. The results obtained in this work suggest that CMT with optimized depositing speed could act as a feasible method to fabricate NiTi alloys. Moreover, good homogeneity of microstructure and properties was obtained, despite of the distinct local mechanical behavior in the lower, middle and upper regions of NiTi walls. Good heat management of the CMT process, together with the optimization of the depositing speed will promote greatly the application of NiTi alloys. The main conclusions of this wok could be summarized as follows:

(1) The combination of torch traveling speed = 30 cm/min and wire feeding speed = 6–7 m/min is obtained for the optimization of depositing speed. With such combination, good wettability between the substrate and deposition is obtained, as indicated by the smaller wettability angle, higher width and lower height. Meanwhile, as compared with the wire feeding speed, the torch traveling speed shows more pronounced influence on the depositing process.
(2) The CMT-fabricated NiTi alloys show distinct microstructure with varying wall height. In the lower region, coarse columnar grains are obtained. The columnar grains are refined with the increase of wall height. Finally, an equiaxed microstructure is obtained in the upper region. The Ni_4Ti_3 precipitates are detected in the matrix. The microstructural homogeneity is improved due to the optimization of depositing speed.
(3) The microhardness, critical stress, and elongation of CMT-fabricated NiTi alloys increase monotonously from 256 to 290 HV, from 483 to 643 MPa and from 6.39% to 6.75%, respectively, with the increase of wall height. Despite of such change, the mechanical properties of NiTi walls along the building direction are more homogeneous due to the improved microstructural homogeneity.
(4) The wear resistance of the lower, middle and upper regions of NiTi walls exhibits moderate change. With the increase of wall height, the coefficient of friction decreases gradually from 0.728 to 0.711, from 0.730 to 0.701 and from 0.692 to 0.664, respectively, while keeping the load = 5, 10, and 20 N. Re-orientation of residual martensite and stress-induced martensitic transformation are key factors for the wear performance of NiTi alloys. Plastic deformation is the main form of wear, together with wear-induced work hardening, eventually leading to crack nucleation and propagation, which is hindered mainly by the superelasticity of NiTi alloys.
(5) The recoverable strain and recovery ratio under 10 loading cycles increase moderately from 2.98% to 3.06% and from 56.44% to 66.51%, respectively with the increase of wall height. Nevertheless, the homogeneity of superelasticity and shape memory property of CMT-fabricated NiTi alloys, along the building direction, is improved by optimizing the depositing speed.

Declaration of Competing Interest

The authors declare that they have no known competing financial interests or personal relationships that could have appeared to influence the work reported in this paper.

Acknowledgements

This work is supported by National Natural Science Foundation of China (Grant 52025053) and the Research Funds from Jiangsu Xuzhou Construction Machinery Research Institute Co., Ltd. (No. HT069-2021).

REFERENCES

[1] Mohd Jani J, Leary M, Subic A, Gibson MA. A review of shape memory alloy research, applications and opportunities. Mater Des 2014;56:1078–113.
[2] Wang Z, Chen J, Besnard C, Korsunsky AM. Microstructure evolution in a severely cold-worked NiTi wire during ageing treatment: an in situ neutron diffraction study. Mater Lett 2020;281:128676.
[3] Sun D, Jiang S, Xing X, Yan B, Yu J, Zhang Y. Microstructures and mechanical properties of equiatomic NiTi shape memory alloy undergoing local canning compression and subsequent annealing. Met Mater Int. 2021;27(12):4901–10.
[4] Elahinia M, Shayesteh Moghaddam N, Taheri Andani M, Amerinatanzi A, Bimber BA, Hamilton RF. Fabrication of NiTi through additive manufacturing: a review. Prog Mater Sci. 2016;83:630–63.

[5] Wang X, Yu J, Liu J, Chen L, Yang Q, Wei H, et al. Effect of process parameters on the phase transformation behavior and tensile properties of NiTi shape memory alloys fabricated by selective laser melting. Addit Manuf. 2020;36:101545.
[6] Hamilton RF, Bimber BA, Palmer TA. Correlating microstructure and superelasticity of directed energy deposition additive manufactured Ni-rich NiTi alloys. J Alloys Compd. 2018;739:712–22.
[7] Li S, Hassanin H, Attallah MM, Adkins NJE, Essa K. The development of TiNi based negative Poisson's ratio structure using selective laser melting. Acta Mater 2016;105:75–83.
[8] Saedi S, Moghaddam NS, Amerinatanzi A, Elahinia M, Karaca HE. On the effects of selective laser melting process parameters on microstructure and thermomechanical response of Ni-rich NiTi. Acta Mater 2018;144:552–60.
[9] Zhou Q, Hayat MD, Chen G, Cai S, Qu X, Tang H, et al. Selective electron beam melting of NiTi: microstructure, phase transformation and mechanical properties. Mater Sci Eng 2019;744:290–8.
[10] Wang J, Pan Z, Wang Y, Wang L, Su L, Cuiuri D, et al. Evolution of crystallographic orientation, precipitation, phase transformation and mechanical properties realized by enhancing deposition current for dual-wire arc additive manufactured Ni-rich NiTi alloy. Addit Manuf. 2020;34:101240.
[11] Wang J, Pan Z, Yang G, Han J, Chen X, Li H. Location dependence of microstructure, phase transformation temperature and mechanical properties on Ni-rich NiTi alloy fabricated by wire arc additive manufacturing. Mater Sci Eng, A 2019;749:218–22.
[12] Ke WC, Oliveira JP, Cong BQ, Ao SS, Qi ZW, Peng B, et al. Multi-layer deposition mechanism in ultra high-frequency pulsed wire arc additive manufacturing (WAAM) of NiTi shape memory alloys. Addit Manuf. 2022;50:102513.
[13] Resnina N, Palani IA, Belyaev S, Prabu SSM, Liulchak P, Karaseva U, et al. Structure, martensitic transformations and mechanical behaviour of NiTi shape memory alloy produced by wire arc additive manufacturing. J Alloys Compd. 2021;851:156851.
[14] Yu L, Chen KY, Zhang YL, Liu J, Yang L, Shi YS. Microstructures and mechanical properties of NiTi shape memory alloys fabricated by wire arc additive manufacturing. J Alloys Compd. 2021;892:162193.
[15] Zhang MG, Fang XW, Wang Y, Jiang X, Chang TX, Xi NY, et al. High superelasticity NiTi fabricated by cold metal transfer based wire arc additive manufacturing. Mater Sci Eng, A 2022;840:143001.
[16] Yang D, Wang G, Zhang G. Thermal analysis for single-pass multi-layer GMAW based additive manufacturing using infrared thermography. J Mater Process Technol. 2017;244:215–24.
[17] Wang J, Pan Z, Carpenter K, Han J, Wang Z, Li H. Comparative study on crystallographic orientation, precipitation, phase transformation and mechanical response of Ni-rich NiTi alloy fabricated by WAAM at elevated substrate heating temperatures. Mater Sci Eng A. 2021;800:140–307.
[18] Kelly SM, Kampe SL. Microstructural evolution in laser-deposited multilayer Ti-6Al-4V builds: part II. Therm Model. 2004;35(6):1869–79.
[19] Otsuka K, Ren X. Physical metallurgy of Ti–Ni-based shape memory alloys. Prog Mater Sci. 2005;50:511–678.
[20] Gu D. In-situ formation of Ni_4Ti_3 precipitate and its effect on pseudoelasticity in selective laser melting additive manufactured NiTi-based composites. Appl Surf Sci 2018;441:826–70.
[21] Liu S, Lin Y, Wang G, Wang X. Effect of varisized Ni_4Ti_3 precipitate on the phase transformation behavior and functional stability of Ti-50.8 at.% Ni alloys. Mater Char. 2021;172:110832.
[22] Solberg JK, Nes E. On the micromechanisms of repeated precipitation on edge dislocations. J Mater Sci. 1978;13:2233–40.
[23] Wang J, Pan ZX, Yang GS, Han J, Chen XZ, Li HJ. Location dependence of microstructure, phase transformation temperature and mechanical properties on Ni-rich NiTi alloy fabricated by wire arc additive manufacturing. Mater Sci Eng, A 2019;749:218–22.
[24] Halani PR, Shin YC. In situ synthesis and characterization of shape memory alloy nitinol by laser direct deposition. Metall Mater Trans A. 2012;43:650–7.
[25] Qin Q, Peng H, Fan Q, Zhang L, Wen Y. Effect of second phase precipitation on martensitic transformation and hardness in highly Ni-rich NiTi alloys. J Alloy Compd 2018;739:873–81.
[26] Frenzel J, Zhang Z, Somsen C, Neuking K, Eggeler G. Influence of carbon on martensitic phase transformations in NiTi shape memory alloys. Acta Mater 2007;55:1331–41.
[27] Frenzel J, George EP, Dlouhy A, Somsen C, Wagner MF-X, Eggeler G. Influence of Ni on martensitic phase transformations in NiTi shape memory alloys. Acta Mater 2010;58:3444–58.
[28] Huang K, Marthinsen K, Zhao Q, Loge RE. The double-edge effect of second-phase particles on the recrystallization behaviour and associated mechanical properties of metallic materials. Prog Mater Sci. 2018;92:284–359.
[29] Oliveira JP, Braz Fernandes FM, Schell N, Miranda RM. Martensite stabilization during superelastic cycling of laser welded NiTi plates. Mater Lett 2016;171:273–6.
[30] Yu ZL, Xu ZZ, Guo YT, Sha PW, Liu RY, Xin RL, et al. Analysis of microstructure, mechanical properties, wear characteristics and corrosion behavior of SLM-NiTi under different process parameters. J Manuf Process. 2022;75:637–50.
[31] Lin PY, Zhu YF, Zhou H, Wang CT, Ren LQ. Wear resistance of a bearing steel processed by laser surface remelting cooled by water. Scripta Mater. 2010;63:839–42.